SIMPLE MULTISPECTRAL IMAGE ANALYSIS FOR SYSTEMICALLY DISEASED CHICKEN IDENTIFICATION

C.−C. Yang, K. Chao, Y. R. Chen, M. S. Kim, H. L. Early

ABSTRACT. *A simple multispectral differentiation method for the identification of systemically diseased chickens was developed and demonstrated. Color differences between wholesome and systemically diseased chickens were used to select interference filters at 488, 540, 580, and 610 nm for the multispectral imaging system. Over a period of 6 months, 660 chicken images were collected in three batches. An image processing algorithm to locate the region of interest (ROI) was developed in order to define four classification areas on each image: whole carcass (WC), region of interest (ROI), upper region (UR), and lower region (LR). Three feature types, average intensity (AI), average normalization (AN), and average difference normalization (ADN), were defined using several wavebands for a total of 12 classification features. A decision tree algorithm was used to determine threshold values for each of the 12 classification features in each of the four classification areas. The AI feature type was found to identify wholesome and systemically diseased chickens better than the AN and ADN features types. Classification by AI in the ROI area, using the 540 and 580 nm wavebands, achieved the best accuracies. AI_{540} achieved 96.3% and 97.1% classification accuracies for wholesome and systemically diseased chickens, respectively. AI_{580} achieved 96.3% and 98.6% classification accuracies for wholesome and systemically diseased chickens, respectively. This simple differentiation method shows potential for automated on−line chicken inspection.*

Keywords. *Food safety, Image classification, Machine vision, Region of interest, Poultry.*

The Food Safety and Inspection Service (FSIS) of the USDA has implemented the Hazard Analysis and Critical Control Point (HACCP) system in poultry plants to improve food safety and prevent food safety hazards in the inspection process (USDA, 1996). FSIS is also testing the proposed HACCP−based Inspection Models Project (HIMP) in a small number of volunteer poultry processing plants to determine if FSIS inspectors and resources can be used more effectively for the poultry inspection program. Performance standards are set at zero tolerance for two Food Safety (FS) categories (i.e., fecal contamination and infectious condition such as septicemia and toxemia) and five non−safety Other Consumer Protection (OCP) categories under HIMP. For poultry plants to meet government food safety regulations and satisfy consumer demand while maintaining their competitiveness, FSIS has recognized the need for new inspection technologies (USDA, 1985), such as automated computer imaging inspection systems.

Recent research has investigated the development of automated poultry inspection techniques based on spectral imaging. Chao et al. (2002) developed a multispectral imaging system using 540 and 700 nm wavelengths and obtained accuracies of 94% for wholesome and 87% for unwholesome chicken carcasses. Through hyperspectral imaging, Park et al. (2002) achieved 97.3% to 100% accuracy in identifying fecal and ingesta contamination of poultry carcasses using images at the 434, 517, 565, and 628 nm wavelengths. These studies found that spectral images present spectral and spatial information from the surface of chicken carcass, which is essential for efficient identification of contaminated and systemically diseased chickens. Not only can multispectral imaging achieve high classification accuracies, this non−destructive method also shows potential for on−line inspections at high−speed processing plants.

Based on visible/near−infrared spectroscopy analysis, previous studies have also shown that certain wavelengths are particularly useful for the identification of diseased, contaminated, or defective chicken carcasses (Chen and Massie, 1993; Chao et al., 2003; Windham et al., 2003). After selection of key wavelengths, filters corresponding to those wavelengths can be implemented for acquisition of multispectral images. Image processing algorithms are then developed to enhance and analyze the images. With appropriate image processing procedures, some features can be extracted from multispectral images to more suitably represent the classification target and increase the classification accuracy.

The main objective of this study was to develop a simple method for differentiation of wholesome and systemically diseased chickens based on multispectral images. The

Article was submitted for review in July 2004; approved for publication by the Information & Electrical Technologies Division of ASABE in December 2005.

Mention of trade names or commercial products is solely for the purpose of providing specific information and does not imply endorsement or recommendation by the USDA.

The authors are **Chun−Chieh Yang, ASABE Member Engineer,** Postdoctoral Scholar, Department of Biosystems and Agricultural Engineering, University of Kentucky, Lexington, Kentucky; **Kuanglin Chao,** Research Scientist, and **Yud−Ren Chen, ASABE Member Engineer,** Research Leader, and **Moon S. Kim,** Research Scientist, USDA−ARS Instrumentation and Sensing Laboratory, Beltsville, Maryland; and **Howard L. Early,** Veterinary Medical Officer, USDA−FSIS, Washington, D.C. **Corresponding author:** Kuanglin Chao, USDA−ARS Instrumentation and Sensing Laboratory, Bldg. 303, BARC−East, 10300 Baltimore Ave., Beltsville, MD 20705−2350; phone: 301−504−8450; fax: 301−504−9466; e−mail: chaok@ba.ars.usda.gov.

wavebands for four filters were selected using analysis of chicken spectra in the visible region. Image processing algorithms were developed to extract image features that were then used to develop differentiation thresholds for the identification of systemically diseased chickens. Independent images were then used to test the differentiation models.

Materials and Methods

Sample Collection

Eviscerated chicken carcasses were identified and collected by USDA−FSIS veterinarians from Allen Family Foods (Cordova, Md.). A total of 660 chicken carcasses were collected in three batches over a period of six months in 2003 and 2004, of which 328 were systemically diseased and 332 were wholesome carcasses. In the first batch, 117 wholesome and 131 systemically diseased birds were collected; in the second batch, 134 wholesome and 127 systemically diseased birds were collected; and in the third batch, 81 wholesome and 70 systemically diseased birds were collected. Systemically diseased birds showed external symptoms of septicemia or toxemia. Septicemia is caused by the presence of pathogenic microorganisms or their toxins in the bloodstream, and toxemia is the result of toxins produced from cells at a localized infection or from the growth of microorganisms.

Chicken carcasses were placed in plastic bags, stored in coolers, and covered with ice to minimize dehydration. Then the bags were transported to the USDA−ARS Instrumentation and Sensing Laboratory (ISL) located in Beltsville, Maryland, within 2 h for the experiments.

Experimental Systems

Vis/NIR Spectroscopic System

An Andor DV401−BV (Andor Technology, Belfast, Northern Ireland) charge−coupled device (CCD) system, consisting of a thermoelectrically cooled 1024 × 127 array detector, was used with the manufacturer's software to acquire chicken sample spectra. Chicken samples were illuminated by an external illumination assembly (model 6000, Spectra−Physics, Stratford, Conn.) consisting of a 100 W quartz tungsten halogen (QTH) filament lamp and a condensing lens (*f* 1.8, 33 mm aperture) to collimate the QTH light. A focusing assembly (model 77799, Spectra−Physics, Stratford, Conn.) was used to focus the collimated light at one end of a bifurcated fiber optic probe (C Technologies, Inc., Cedar Knolls, N.J.). The probe consisted of two concentric groups of fiber optic bundles. The fibers of the outer bundle transmitted the focused light to illuminate the chicken surface from a distance of 20 mm. The fibers of the inner optic bundle, each 100 μm in diameter, returned reflected light to the CCD detector.

Multispectral Imaging System

The multispectral imaging system consisted of a MultiSpec Imager imaging spectrograph (Optical Insights, LLC, Santa Fe, N.M.), a SpectraVideo SV 512 back−illuminated CCD camera (PixelVision, Inc., Tigard, Ore.), a PMB−004 shutter and cooler control board, a PMB−007 serial interface board, a PMJ−002 PCI bus data acquisition board, a LynxPCI frame grabber, a Pentium III 600 PC computer (Gateway, Poway, Cal.), and four 100 W tungsten halogen lights. Four interference filters and an optical mirror assembly were used to create four waveband images of the target that were acquired simultaneously on a single CCD focal plane. The resulting 16−bit multispectral image contained four sub−images. The PixelView version 3.20 utility program (PixelVision, Inc., Tigard, Ore.) was used to control camera settings, such as integration time and image acquisition.

Vis/NIR Spectrum Measurement

The CCD spectroscopic system was used to collect spectral measurements for 100 wholesome and 80 systemically diseased carcasses. The system was wavelength−calibrated using several emission peaks (435.84, 546.07, 640.23, and 724.52 nm) from a high−intensity mercury neon lamp before spectral measurements were taken. A dark reference was taken with the light source turned off to compensate for the zero energy signals. A white reference measurement was taken by placing the fiber optic probe 20 mm from a 14 mm thick piece of Spectralon reflectance target (Labsphere, Sutton, N.H.). Spectra were recorded as relative reflectance relative to the light reflected from the Spectralon reflectance target, i.e.:

$$\text{Relative Reflectance} = \frac{\text{Sample reflectance} - \text{Dark reference}}{\text{White reference} - \text{Dark reference}} \quad (1)$$

The distance from the fiber optic probe to the sample was 20 mm. Each spectrum was measured by a single scan with an exposure time of 120 ms. Each spectrum had 1024 data points from 401.02 nm to 866.67 nm spaced 0.455 nm apart.

Determination of the Bandpass Filters

The mean color differences (between wholesome and systemically diseased birds) in CIELAB color space were used to determine appropriate bandpass filters for the multispectral imaging system. The International Committee on Illumination (CIE) tristimulus values *X*, *Y*, and *Z* of the color of a sample were obtained by multiplying the spectral irradiance of the light source, the reflectance of the chicken sample, and the 1931 CIE color matching functions $\bar{x}$, $\bar{y}$, and $\bar{z}$. In this study, the CIE tristimulus values were calculated by numerical summation of mean spectra data, for both wholesome and systemically diseased birds, over the wavelengths in the visible spectrum (401 nm to 649 nm with 1 nm intervals):

$$X = k \sum_{\lambda=401}^{649} S(\lambda)\, R(\lambda)\, \bar{x}(\lambda) \quad (2)$$

$$Y = k \sum_{\lambda=401}^{649} S(\lambda)\, R(\lambda)\, \bar{y}(\lambda) \quad (3)$$

$$Z = k \sum_{\lambda=401}^{649} S(\lambda)\, R(\lambda)\, \bar{z}(\lambda) \quad (4)$$

where *k* is a normalizing constant (k = 683 lm W^{-1}), $S(\lambda)$ is the spectral irradiance of the QTH light source (W m^{-2} nm^{-1}), $R(\lambda)$ is the spectral reflectance distribution of the chicken sample, and $\bar{x}$, $\bar{y}$, and $\bar{z}$ are color matching functions.

The CIE tristimulus values were used to calculate the values for *L** (lightness), *a** (redness), and *b** (yellowness) in the CIE 1976 *L*a*b** color space:

$$L^* = 116(Y/Y_n)^{1/3} - 16 \quad (5)$$

$$a^* = 500[(X/X_n)^{1/3} - (Y/Y_n)^{1/3}] \quad (6)$$

$$b^* = 200[(Y/Y_n)^{1/3} - (Z/Z_n)^{1/3}] \quad (7)$$

where X, Y, and Z are tristimulus values of the given light stimulus; X_n, Y_n, and Z_n are tristimulus values of the white reference; and the quotients X/X_n, Y/Y_n, and Z/Z_n are all greater than 0.008856. Note that if any of the quotients had been less than or equal to 0.008856, then a slightly different set of equations would have been used.

The color difference between wholesome and systemically diseased birds in CIELAB space (ΔE) was calculated as the Euclidean distance between the points in this three−dimensional space:

$$\Delta E\left(L^* a^* b^*\right) = \left[\left(\Delta L^*\right)^2 + \left(\Delta a^*\right)^2 + \left(\Delta b^*\right)^2\right]^{1/2} \quad (8)$$

Calculated using equation 8, figure 1 shows the plot of the wavelength−by−wavelength color difference (ΔE) in the visible region from 401 nm to 649 nm. The most significant color differences in the plot occur in the areas of 576, 540, and 440 nm. Despite the significant color difference around 440 nm, a filter was deemed unsuitable in this area due to system limitations. Compared to higher waveband regions, the QTH light source has a lower output in the 440 nm region, but using increased light intensity in this area would result in saturation of the spectral signal in the visible spectral region at longer wavelengths.

The greatest color difference occurred at 576 nm; the closest market−available match was an interference filter centered at 580 nm with 10 nm FWHM (full width at half maximum). Two additional filters were selected based on previous findings (Swatland, 1989; Liu and Chen, 2000, 2001) that identified various forms of myoglobin as major determinants of chicken meat and skin color and associated deoxymyoglobin, oxymyoglobin, and metmyoglobin with specific wavebands at 440, 545, and 485 nm, respectively. Consequently, the filter parameters selected for this study were 10 nm FWHM at 488 nm, 10 nm FWHM at 540 nm, 10 nm FWHM at 580 nm, and 10 nm FWHM at 610 nm. The last, at 610 nm, was used for image masking purposes due to the lower color difference at that waveband between wholesome and systemically diseased chickens.

Multispectral Image Collection and Image Registration

After the wavebands were selected, the chicken carcass images were taken, processed, and differentiated. Figure 2 shows the flowchart for multispectral image registration, processing, and differentiation. The details of the flowchart are described below.

The distance between the camera lens and the chicken sample field of view was 1143 mm. Four tungsten halogen lights were mounted 610 mm from the field of view, on a rectangular frame. During image collection, a Spectralon diffuse reflectance target of 99% reflectance (Labsphere, North Sutton, N.H.) was used as a calibration target for flat−field correction.

Since the image consists of four sub−images (one for each wavelength) acquired simultaneously on the single CCD focal plane, selection of a single integration time that results in a clear image for each channel is essential. The proper integration time was needed to reduce noise in the short−wavelength sub−image (488 nm) and to avoid over−saturation in the long−wavelength sub−image (610 nm) and in flat−field calibration. From trial−and−error tests on some chicken samples, it was found that the multispectral image was safely below saturation level when the integration time was set at 500 ms with high gain setting (approximately 5.5 electrons per analog−to−digital unit). These settings were used for both flat−field calibration and acquisition of the chicken images. The cooling temperature for the camera control unit was set at 251 K.

Calibration and dark reference images were acquired prior to collection of chicken images. The Spectralon reference target with illumination was used for the calibration refer−

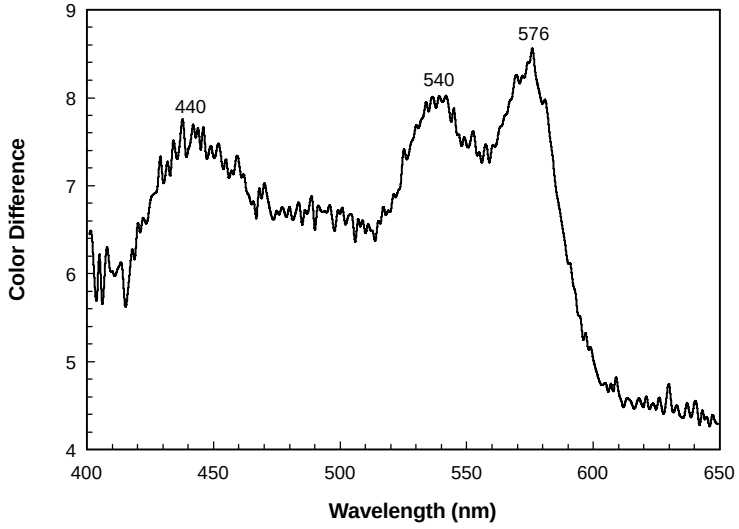

Figure 1. Wavelength−by−wavelength color difference between mean wholesome chicken spectrum and mean systemically diseased chicken spectrum, showing the most significant color differences in the areas of 576, 540, and 440 nm.

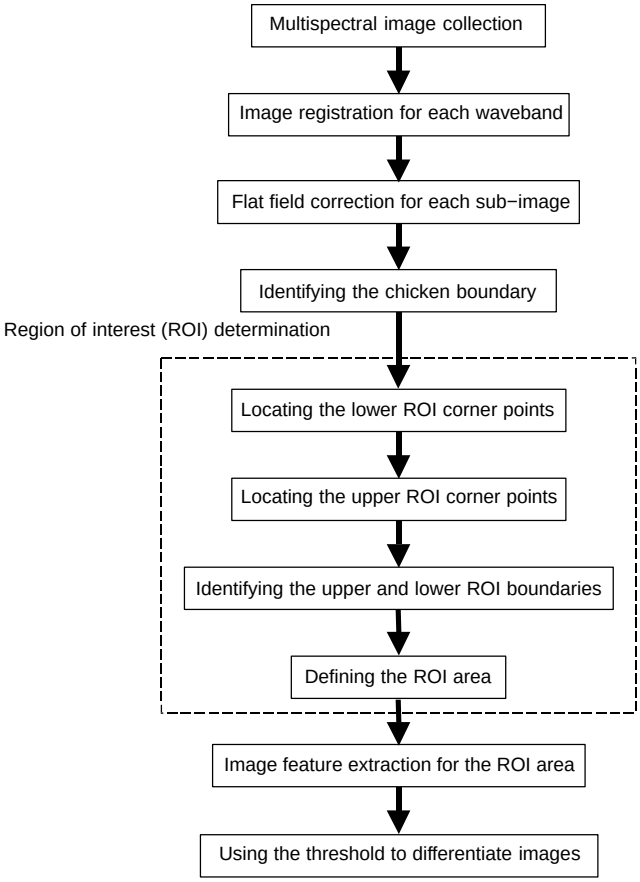

Figure 2. Diagram of image collection, processing, and differentiation for systemically diseased chicken identification.

ence image, and the camera lens was covered for the dark reference image. For each chicken image, the chicken was hung on the shackle against a black background so that the chicken image could be easily extracted from the background.

Each original image consisted of four sub−images at 488, 540, 580, and 610 nm, arranged clockwise from the upper left quadrant; pixel (*x*, *y*) coordinates were defined with (0, 0) in the upper left corner of the image. For image registration, a grid paper with four pre−defined points was used. In an image of the grid paper, each sub−image showed the four points each as one pixel. The 610 nm sub−image in the lower left quadrant, a 214 × 241 pixel area defined by four boundary points at (282, 20), (282, 260), (495, 260), and (495, 20), was used as the base image in determining the offset vectors between the base image and each of the three other sub−images. For example, to determine the offset vector between the base image and the 488 nm sub−image (upper left quadrant), the difference in (*x*, *y*) coordinates was calculated for each of the four points, and the average (rounded to the nearest integer) was taken. The offset vectors were used to determine the boundaries of the other three sub−images corresponding to the boundaries of the base image. The pixel size for each sub−image was 0.93 × 0.93 mm.

Multispectral Image Processing

Four image processing steps were performed, using MATLAB 6.1 (MathWorks, Inc., Natick, Mass.), to obtain single−channel sub−images for image analysis, as diagrammed in figure 3. First, flat−field correction was performed according to the equation:

$$I = \frac{I_0 - B}{W - B} \tag{9}$$

where I_0 is the original image, B is the dark reference image, W is the white Spectralon reference image, and I is the relative reflectance image. Second, the 610 nm sub−image was located and used to build a mask. On the 610 nm sub−image, it was observed that the intensity for the black background was always below 0.1 and the chicken intensity was always above 0.1. Thus, a threshold value of 0.1 was used to create the mask. Third, the mask was replicated in each quadrant of the image using the vectors of image registration. This mask was applied to the original image to remove the background. This resulted in the background pixels of each image being reset to zero; for other pixels, the intensity values remained the same. Last, the four sub−images were separated using the vectors of image registration.

After the sub−images were obtained, intensity contour maps were generated for analysis. Figure 4 shows contour maps of a wholesome chicken and a systemically diseased chicken. It is evident that the major differences between wholesome and systemically diseased chicken occur between the breast and lower abdomen. Therefore, for proper identification of systemically diseased chickens from wholesome chickens, the region of interest (ROI) was defined around this area. The image area above the ROI was termed "upper region" (UR) and included the upper breast and

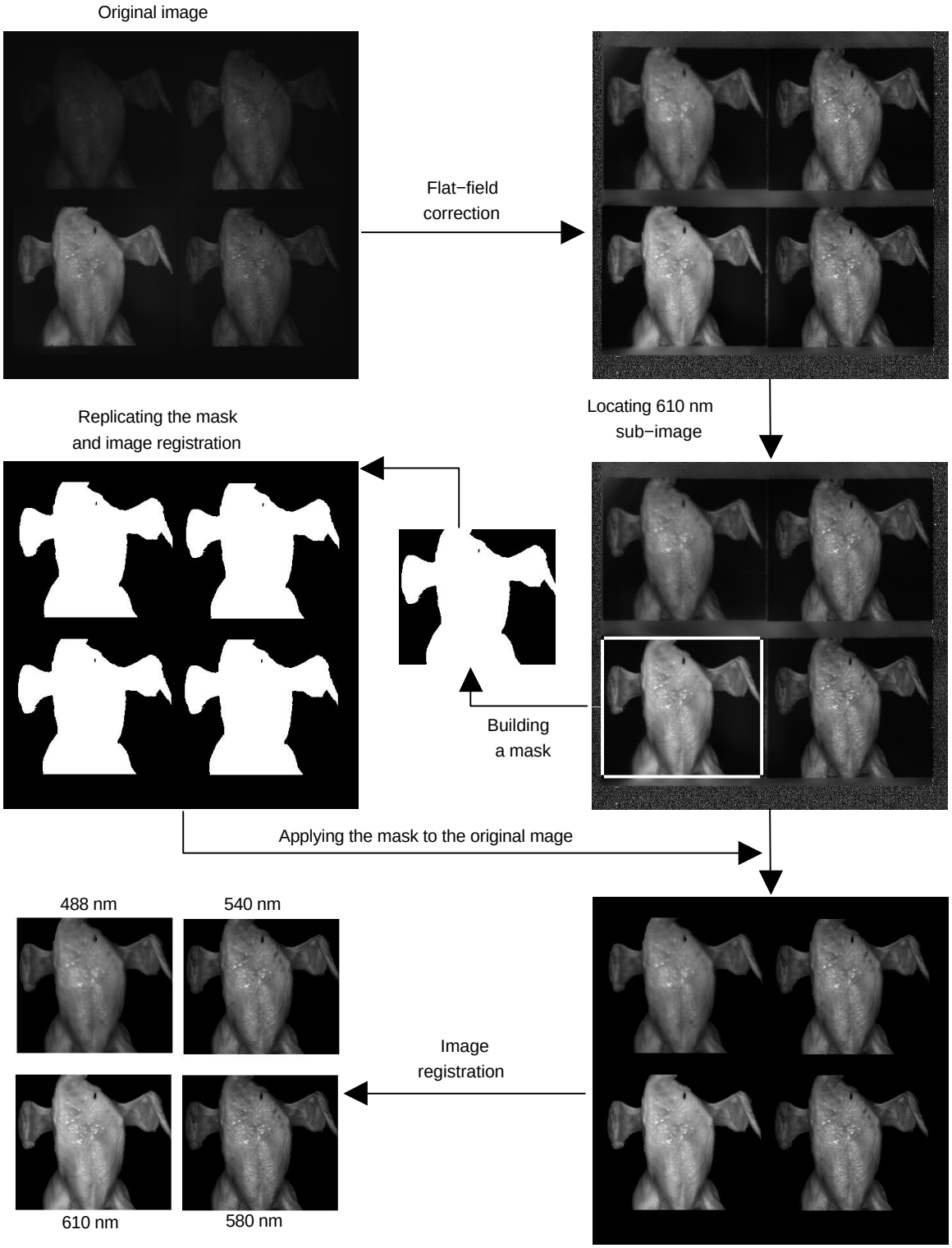

Figure 3. Image processing to obtain single−channel sub−images.

wings. The image area under the ROI was termed “lower region” (LR) and included the lower abdomen and thighs. The area of the whole carcass (WC) consists of the ROI, UR, and LR.

To find the ROI boundaries on an image, four corner points must be located. The lower left and lower right corner points were the conjunction points between abdomen and thigh along the chicken boundary. The upper left and upper right corner points were the conjunction points between abdomen and wing along the chicken boundary. Figure 5 shows an example of the four corner points defining the ROI on a chicken image. Using the mask image created from the 610 nm sub−image, the boundary of the chicken carcass was identified. As shown in figure 6, the lowest point of the boundary, which was on the thigh, was then located as the start point P_1. From this start point along the boundary, seven

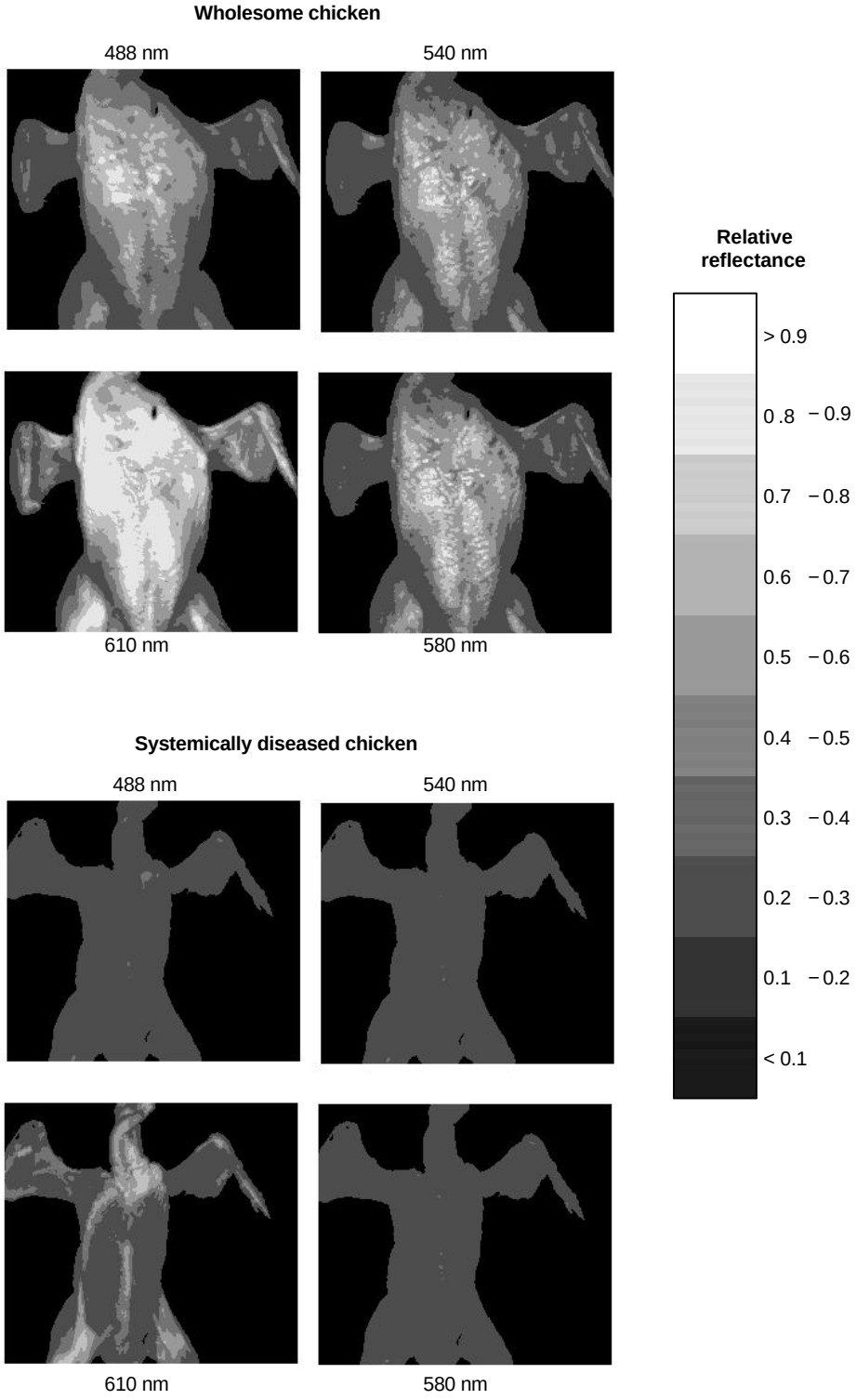

Figure 4. Contour images showing relative reflectance for wholesome and systemically diseased chickens.

points were located, noted as $P_1(x_1, y_1)$ to $P_7(x_7, y_7)$. Because the boundary was formed by discrete pixels (points) instead of a continuous line, the distance d was determined by trial and error. The distance d where $d = x_i - x_{i-1}$ was six pixels, or approximately 5.58 mm. It was found that the corner point would be missed if the distance d were shorter or longer than six pixels. The following relational and logical operations were carried out:

$$A_L = \{(y_{j+1} - y_j \geq 0) \text{ and } (y_{j+2} - y_{j+1} \geq 0) \text{ and } (y_{j+3} - y_{j+2} \geq 0)\} \quad (10)$$

$$B_L = \{(y_{j+3} - y_{j+4} \geq 0) \text{ and } (y_{j+4} - y_{j+5} \geq 0) \text{ and } (y_{j+5} - y_{j+6} \geq 0)\} \quad (11)$$

$$C_L = \{(y_{j+3} - y_{j+4} \leq 0) \text{ and } (y_{j+4} - y_{j+5} \leq 0) \text{ and } (y_{j+5} - y_{j+6} \leq 0)\} \quad (12)$$

$$D_L = \{(y_{j+3} - y_{j+4} < y_{j+4} - y_{j+5}) \text{ and } (y_{j+4} - y_{j+5} < y_{j+5} - y_{j+6})\} \quad (13)$$

$$T_L = \{(A_L) \text{and} [(B_L) \text{or} ((C_L) \text{and} (D_L))]\} \quad (14)$$

Empirically, the logical value of T_L was true only at the conjunction point between chicken thigh and abdomen. When the value of T_L was true, the point P_4 was determined to be the lower left corner point. Otherwise, the point at the boundary line and adjacent to the start point P_1 was selected as the new start point, and thus another seven points were located to repeat the above operations. Similarly, the following relational and logical operations were carried out to determine the lower right corner point:

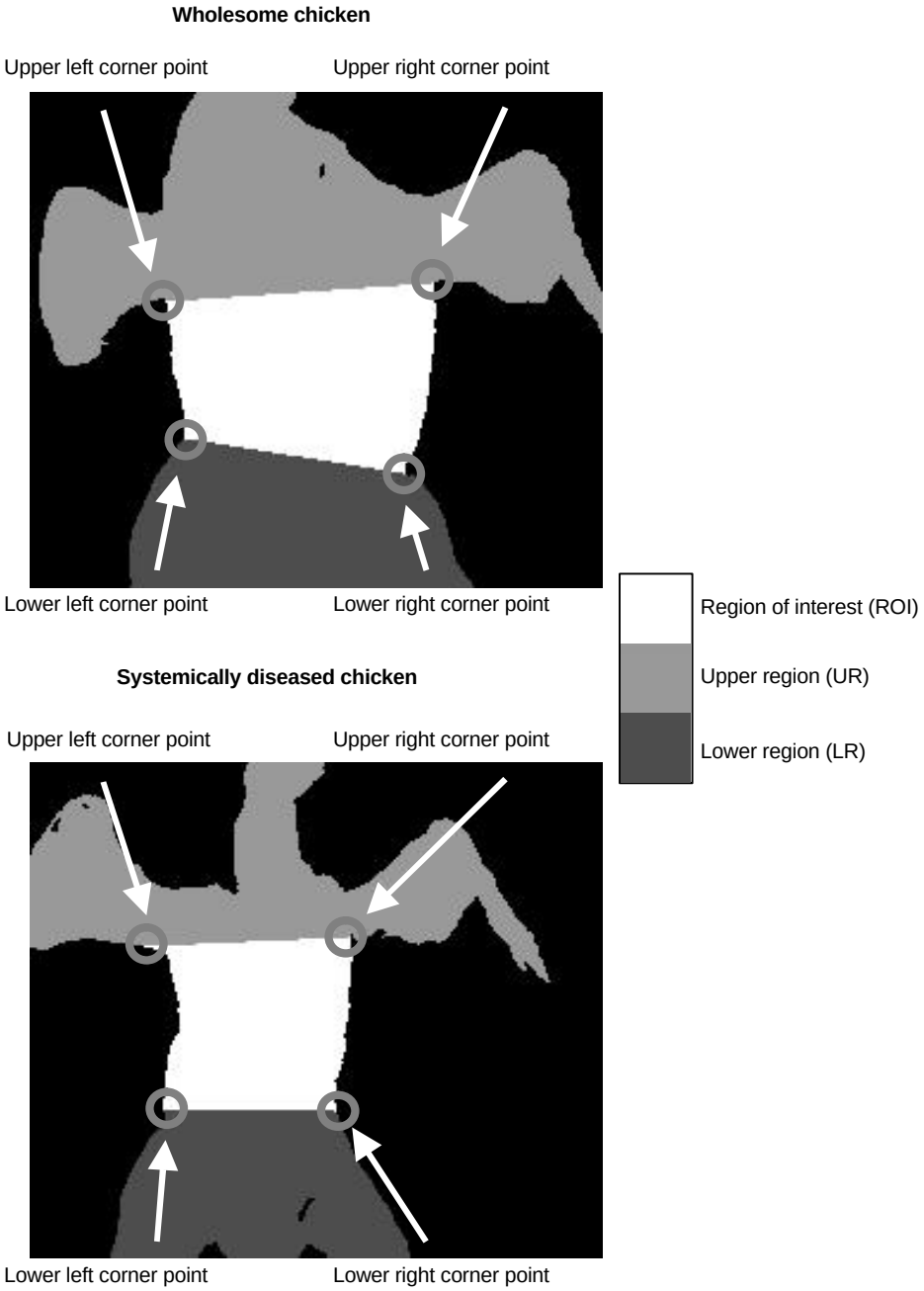

Figure 5. Definition of classification areas by ROI corner points.

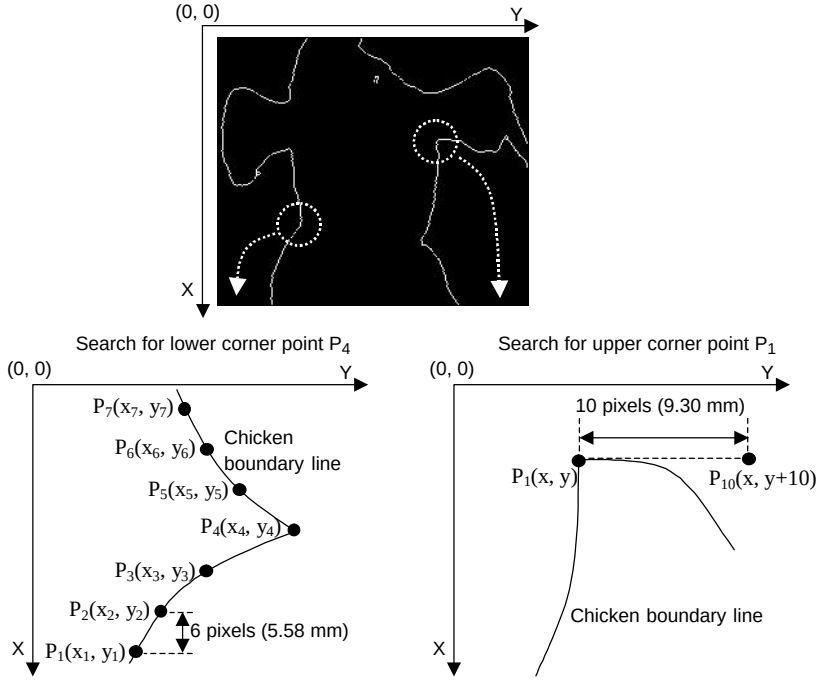

Figure 6. Search operation for the ROI corner points.

$$A_R = \{(y_{j+1} - y_j \le 0) \text{ and } (y_{j+2} - y_{j+1} \le 0) \text{ and } (y_{j+3} - y_{j+2} \le 0)\} \quad (15)$$

$$B_R = \{(y_{j+3} - y_{j+4} \le 0) \text{ and } (y_{j+4} - y_{j+5} \le 0) \text{ and } (y_{j+5} - y_{j+6} \le 0)\} \quad (16)$$

$$C_R = \{(y_{j+3} - y_{j+4} \ge 0) \text{ and } (y_{j+4} - y_{j+5} \ge 0) \text{ and } (y_{j+5} - y_{j+6} \ge 0)\} \quad (17)$$

$$D_R = \{(y_{j+3} - y_{j+4} > y_{j+4} - y_{j+5}) \text{ and } (y_{j+4} - y_{j+5} > y_{j+5} - y_{j+6})\} \quad (18)$$

$$T_R = \{(A_R) \text{and} [(B_R) \text{or} ((C_R) \text{and} (D_R))]\} \quad (19)$$

The operations were repeated until the logical value of T_R was true, at which the point P_4 was then determined as the lower right corner point.

From the lower left corner point $P_L(x_i, y_j)$, the point $P_1(x_i - i, y_k)$ in the boundary line was located, and ten pixels (approximately 9.30 mm) from $P_1(x_i - i, y_k)$ to $P_{10}(x_i - i, y_k - 9)$ were compared to the chicken boundary. This operation was repeated until ten pixels from P_1 to P_{10} were all within the chicken boundary, which indicated the starting point of the chicken wing. Therefore, the point P_1 would be determined as the upper left corner point. Similarly, from the lower right corner point $P_R(x_i, y_j)$, the point $P_1(x_i - 1, y_k)$ in the boundary line was located, and ten pixels from $P_1(x_i - 1, y_k)$ to $P_{10}(x_i - 1, y_k + 9)$ were compared to the chicken boundary. This operation was repeated until ten pixels from P_1 to P_{10} were all within the chicken boundary, so that the point P_1 was determined as the upper right corner point. Figure 6 illustrates the search operation for the ROI corner points.

After the four corner points were located, the straight line between the two upper corner points and the straight line between the two lower corner points defined the upper and lower boundaries of the ROI, respectively. The right and left ROI boundaries were defined by segments of the chicken boundary lines between the two right corner points and two left corner points.

Threshold Generation

Four classification areas on each image were defined using the ROI, UR, LR, and WC areas. Three image feature types were calculated: average intensity (AI), average normalization (AN), and average difference normalization (ADN). For AI, the average intensity was calculated for each area. The AN value was the average of the ratio of intensity between two wavelengths at each pixel in the area. The ADN value was the average of the difference normalization of intensity between two wavelengths at each pixel in the area. The calculations for $AN_{fi\,/\,fj}$ and $ADN_{fi\,/\,fj}$ between the sub−images I at the wavelengths fi and fj were as follows:

$$AN_{fi/fj} = \frac{I_{fi}}{I_{fj}} \quad (20)$$

$$ADN_{fi/fj} = \frac{I_{fi} - I_{fj}}{I_{fi} + I_{fj}} \quad (21)$$

Four pairs of wavelengths were used for AN and ADN: I_{488}/I_{610}, I_{540}/I_{610}, I_{580}/I_{610}, and I_{540}/I_{580}. Twelve features (combining feature type and wavelength) were calculated in each of the four areas, for a total of 48 classification features for each image.

After the first batch of 117 wholesome and 131 systemically diseased chicken images was collected, the Classification and Regression Trees (CART) decision tree statistic algorithm (Breiman et al., 1984) was used to generate a threshold to differentiate wholesome and systemically diseased chickens for each of the 48 features, using the AnswerTree 3.0 program (SPSS, Chicago, Ill.). CART was selected because this algorithm has been applied successfully to data classification (Balk and Elder, 2000; Eisenberg and McKone, 1998; Pietersma et al., 2003; Yang et al., 2004). The maximum tree level was set at one to obtain the threshold. After obtaining the thresholds for the 48 features, the classification accuracies for each feature were examined and the features with the highest accuracies were selected for testing on the second batch of 134 wholesome and 127 systemically diseased chicken images. Thresholds for the 48 features were then updated using the combined data of both first and second batches, and were tested for differentiation of the 81 wholesome and 70 systemically diseased chicken images in the third batch. These results were then compared to differentiation results obtained using the original thresholds tested on the third batch of chicken images.

Results and Discussion

Table 1 summarizes significance t−test results for comparing CIELAB values from wholesome and systemically diseased chicken samples. The mean lightness value (L) of the wholesome chickens was higher than that of systemically diseased chickens. The mean redness value (a*) of the wholesome chickens was lower than that of systemically diseased chickens. However, no significant difference was found between wholesome and systemically diseased chicken samples when the mean yellowness value (b*) was compared. CIELAB values of these samples suggested that the systemically diseased chickens were darker (lower L*) and redder (higher a*) than wholesome chickens.

Table 2 shows the classification accuracies of the 48 features for the first batch of chicken images. The highest classification accuracies resulted from using the average intensity (AI) in the ROI and WC areas; among these, the 540 and 580 nm performed best. Therefore, thresholds for the AI feature type, at 540 and 580 nm in both the ROI and WC areas, were selected for testing on the second batch of images. At both wavebands, the AI threshold was found to classify better for the WC area, as seen in table 3, with AI_{540} classification accuracies of 98.5% and 97.6% for wholesome and systemically diseased images, respectively, and AI_{580} classification accuracies of 100.0% and 96.1% for wholesome and systemically diseased images, respectively.

Table 4 shows the classification results of using the combined data of the first and second batches to generate the 48 feature thresholds. These results are similar to those shown in table 2. Again, AI is a better feature type for classification than either AN or ADN; higher classification accuracies were achieved using AI in the ROI and WC areas, and in these areas, the 540 and 580 wavebands outperformed the other two wavebands. The AI feature type in these combinations was then tested on the third batch.

Table 1. The International Committee on Illumination L* (lightness), a* (redness), and b* (yellowness) characteristics of wholesome and systemically diseased chickens.[a]

Poultry Carcass Condition	L*	a*	b*
Wholesome	75.08 a	4.15 a	6.23 a
	(0.42)	(0.15)	(0.29)
Systemically diseased	67.99 b	7.50 b	6.64 a
	(0.82)	(0.32)	(0.46)

[a] Means within the same column followed by different letters are statistically different ($P < 0.05$). Values in parentheses are the standard errors of the mean (100 wholesome and 80 systemically diseased chicken samples).

Table 2. Classification accuracies using different poultry carcass regions for the 117 wholesome and 131 systemically diseased chicken images collected in the first batch.

Image Feature	Poultry Carcass Condition	Classification Accuracy (%)			
		Region of Interest	Upper Region	Lower Region	Whole Carcass
AI_{488}[a]	Wholesome	89.7	80.3	83.8	86.3
	Diseased	88.6	89.3	81.7	87.8
AI_{540}	Wholesome	**100.0**[b]	94.9	94.9	**94.0**
	Diseased	**90.8**	92.4	89.3	**97.0**
AI_{580}	Wholesome	**100.0**	94.9	91.5	**96.6**
	Diseased	**92.4**	92.4	92.4	**95.4**
AI_{610}	Wholesome	98.3	94.0	99.2	94.9
	Diseased	87.0	86.3	66.4	89.3
$AN_{488/610}$[c]	Wholesome	57.3	71.8	51.3	57.3
	Diseased	73.3	67.2	87.8	80.2
$AN_{540/610}$	Wholesome	73.5	84.6	91.5	94.9
	Diseased	93.1	90.1	87.8	83.2
$AN_{580/610}$	Wholesome	88.0	98.3	89.7	90.6
	Diseased	83.2	72.5	88.6	86.3
$AN_{540/580}$	Wholesome	77.8	0.0	93.2	88.0
	Diseased	68.7	100.0	30.5	45.0
$ADN_{488/610}$[d]	Wholesome	57.3	71.8	77.8	54.7
	Diseased	73.3	67.9	64.1	82.4
$ADN_{540/610}$	Wholesome	73.5	84.6	91.5	95.7
	Diseased	93.1	89.3	87.0	84.0
$ADN_{580/610}$	Wholesome	88.9	98.3	89.7	84.6
	Diseased	83.2	71.8	89.3	92.4
$ADN_{540/580}$	Wholesome	82.1	90.6	92.3	99.2
	Diseased	64.1	28.2	25.2	19.1

[a] AI_{fi} = average intensity at wavelength fi.
[b] **Bold** numbers indicate the highest classification accuracies.
[c] $AN_{fi/fj}$ = average normalization at wavelengths fi and fj.
[d] $ADN_{fi/fj}$ = average difference normalization at wavelengths fi and fj.

Table 3. Classification accuracies using different poultry carcass regions for the 134 wholesome and 127 systemically diseased chicken images collected in the second batch.

Image Feature	Poultry Carcass Condition	Classification Accuracy	
		Region of Interest	Whole Carcass
AI_{540}[a]	Wholesome	100.0%	**98.5%**[b]
	Diseased	86.6%	**97.6%**
	Threshold	0.2524	**0.2400**
AI_{580}	Wholesome	100.0%	100.0%
	Diseased	89.8%	96.1%
	Threshold	0.2740	0.2415

[a] AI_{fi} = average intensity at wavelength fi.
[b] **Bold** numbers indicate the highest classification accuracies.

Table 4. Classification accuracies using different poultry carcass regions for the 251 wholesome and 258 systemically diseased chicken images collected in the first and second batches.

Image Feature	Poultry Carcass Condition	Classification Accuracy (%)			
		Region of Interest	Upper Region	Lower Region	Whole Carcass
AI_{488}[a]	Wholesome	91.6	84.1	88.1	91.2
	Diseased	85.3	85.7	72.9	82.6
AI_{540}	Wholesome	**96.4**[b]	92.8	95.2	**97.6**
	Diseased	**97.3**	96.9	91.5	**96.1**
AI_{580}	Wholesome	**96.4**	95.6	95.2	**97.6**
	Diseased	**97.7**	93.4	91.1	**97.7**
AI_{610}	Wholesome	96.0	94.4	89.6	94.8
	Diseased	89.2	86.8	78.3	93.4
$AN_{488/610}$[c]	Wholesome	30.3	61.8	70.1	54.6
	Diseased	86.1	72.5	63.2	77.9
$AN_{540/610}$	Wholesome	92.8	85.3	94.0	91.6
	Diseased	81.0	91.9	91.1	89.9
$AN_{580/610}$	Wholesome	94.4	84.5	93.2	92.8
	Diseased	82.2	90.3	90.7	88.4
$AN_{540/580}$	Wholesome	78.1	100.0	82.0	85.7
	Diseased	51.2	5.8	36.8	42.3
$ADN_{488/610}$[d]	Wholesome	30.7	60.6	72.5	53.4
	Diseased	86.1	74.0	62.0	78.7
$ADN_{540/610}$	Wholesome	90.8	87.7	94.0	96.4
	Diseased	83.3	90.3	91.1	84.5
$ADN_{580/610}$	Wholesome	94.8	92.4	93.2	92.0
	Diseased	82.6	81.0	91.1	89.5
$ADN_{540/580}$	Wholesome	92.8	98.4	93.2	91.6
	Diseased	31.4	9.3	18.2	27.5

[a] AI_{fi} = average intensity at wavelength *fi*.
[b] **Bold** numbers indicate the highest classification accuracies.
[c] $AN_{fi/fj}$ = average normalization at wavelengths *fi* and *fj*.
[d] $ADN_{fi/fj}$ = average difference normalization at wavelengths *fi* and *fj*.

Table 5 shows the results of using the original and updated thresholds for the selected AI feature type at 540 and 580 nm in both the ROI and WC areas. The best classification accuracies were achieved using the updated threshold for AI_{580} in the ROI area, with 96.3% and 98.6% for wholesome and systemically diseased chicken images, respectively. The classification accuracies achieved using the updated threshold for AI_{540} in the ROI area are similarly high, with 96.3% and 97.1% for wholesome and systemically diseased chicken images, respectively.

Overall, the AI classification features (using single−waveband average intensities) performed better than the AN and ADN features (using band ratios) for the particular wavebands at 488, 540, 580, and 610 nm. In examining color differences between wholesome and systemically diseased images at any of one of these wavebands, average wholesome AI is consistently higher than average systemically diseased AI. The wavebands at 540 and 580 nm are known to reflect differences between wholesome and systemically diseased chicken condition (Liu and Chen, 2001). However, the AI values at all of these wavebands change in the same direction when comparing individual chickens, regardless of wholesome or systemically diseased condition, i.e., the band ratios using these particular wavebands show very little variation with chicken condition. The waveband at 610 nm is not known to correspond to changes in chicken condition and thus was chosen for image masking purposes. The AN and ADN features that use this band for normalization with either the 540 or 580 nm waveband show reasonably high classification rates.

Table 5. Classification accuracies using different poultry carcass regions for the 81 wholesome and 70 systemically diseased chicken images collected in the third batch.

Image Feature	Poultry Carcass Condition	Updated Threshold		Original Threshold	
		Region of Interest	Whole Carcass	Region of Interest	Whole Carcass
AI_{540}[a]	Wholesome	96.3%	98.8%	100.0%	97.5%
	Diseased	97.1%	90.0%	81.4%	95.7%
	Threshold	0.2829	0.2337	0.2524	0.2400
AI_{580}	Wholesome	**96.3%**[b]	98.8%	100.0%	98.8%
	Diseased	**98.6%**	92.9%	85.7%	94.4%
	Threshold	**0.3026**	0.2469	0.2740	0.2415

[a] AI_{fi} = average intensity at the wavelength *fi*.
[b] **Bold** numbers indicate the highest classification accuracies.

The results show that AI values at both the 540 and 580 nm wavebands can be useful in differentiating between wholesome and systemically diseased chickens. Between these two wavebands, the 580 nm waveband may perform slightly better for identifying systemically diseased chickens, particularly using the ROI area. As the sample population used for determining threshold values was increased, differentiation using either waveband in the WC area performed reasonably well, but not quite as well as in the ROI area for systemically diseased chickens. Classification rates in the WC area using AI_{540} and AI_{580} decreased by 5.7% and 1.5%, respectively, when additional samples were used to determine the threshold values, as can be seen in table 5. Figures 7 and 8 show the average intensity values for three image batches in the 540 and 580 nm wavebands, respectively.

As shown in figures 7 and 8, AI values in the WC area show slightly more overlap between wholesome and systemically diseased birds than AI values in the ROI area, which appears to result from the inclusion of the UR and LR areas within the WC area. The UR and LR areas contribute a greater number of lower−intensity pixels to the AI calculation for wholesome birds, particularly with the wings in the UR area and thighs in the LR area, as can be seen in the contour images in figure 4. The updated threshold values in the WC area changed only by −0.0063 and +0.0054 for AI_{540} and AI_{580}, respectively, but these small changes caused significant differences in the systemically diseased accuracy rates.

When using the ROI differentiation thresholds originally determined from the first batch of sample images, the AI_{540} and AI_{580} systemically diseased classification accuracies for samples in the third batch were lower (81.4% and 85.7%, respectively) than the wholesome classification accuracies of 100%. After thresholds were updated using samples from the combined first and second batches, the AI_{540} and AI_{580} systemically diseased classification accuracies for samples in the third batch improved significantly to 97.1% and 98.6%, respectively. Examination of the data found that in the first batch of sample images, as shown in figures 7 and 8, the AI values for systemically diseased samples in the ROI area showed a few isolated systemically diseased samples in the high−intensity range overlapping with the low−intensity range of the wholesome AI values. The AI_{540} and AI_{580} ROI differentiation thresholds determined from this set of data were thus slightly lower than the thresholds subsequently determined from the combined first and second batches of

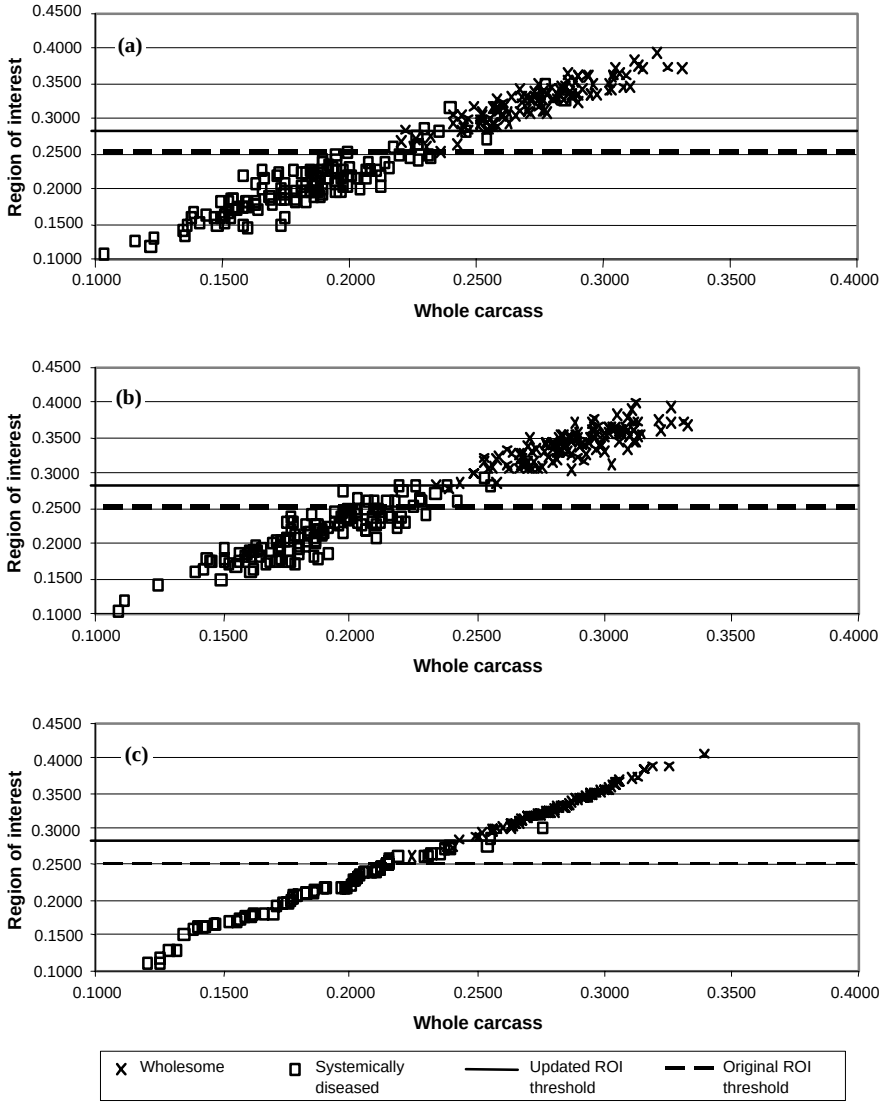

Figure 7. Average intensity values in the 540 nm waveband for (a) the first image batch, (b) the second image batch, and (c) the third image batch.

sample images. The combined data used to update the thresholds thus accounts for the improvement observed in the septicemia classification rates using the updated thresholds.

In addition to the high AI_{540} and AI_{580} classification accuracies obtained using the ROI area, illumination factors affecting chicken sample presentation also make the ROI area more feasible for inspection based on image analysis methods than the WC, UR, and LR areas. In presenting a bird for image acquisition, providing uniform illumination across the entire chicken carcass is a great challenge. In any practical setup, shadows will always occur on peripheral areas of the carcass, such as the wings, thighs, and sides of the bird. Spectral features from the chicken breast area are least affected by physical shape, and thus variations in intensity are predominantly due to actual differences in the sample condition. Although some simpler ROI location methods could have been used, such as locating an arbitrarily sized ROI centered around the centroid of the bird or a maximized rectangular ROI within the boundaries of the chicken breast area, the ROI determined by locating corner points of the breast region was used in this study to maximize the area on the chicken breast that could be used for classification while excluding known areas of difficulty.

A single waveband filter at either 580 nm or 540 nm, and one additional filter at a longer waveband for image masking purposes (e.g., 610 nm) could be implemented for identification of systemically diseased chickens by an automated online multispectral imaging system using the simple AI calculation. By comparing the results in tables 3 and 5 with previously reported results (Chao et al., 2002; Park et al., 2002), the classification accuracy of the method in this study is satisfactory. In determining the classification thresholds, only one image feature at a time was presented to CART and the resulting data always formed two clusters. Consequently, only one threshold was determined for each image feature, resulting in the use of CART with only one level. Although this is a simplified use of CART, the method can be easily implemented for generating new decision thresholds online when chicken carcass variations are expected or when the classification criteria are modified, such as by using multiple image features for classification instead of a single image feature, for identification of systemically diseased chickens.

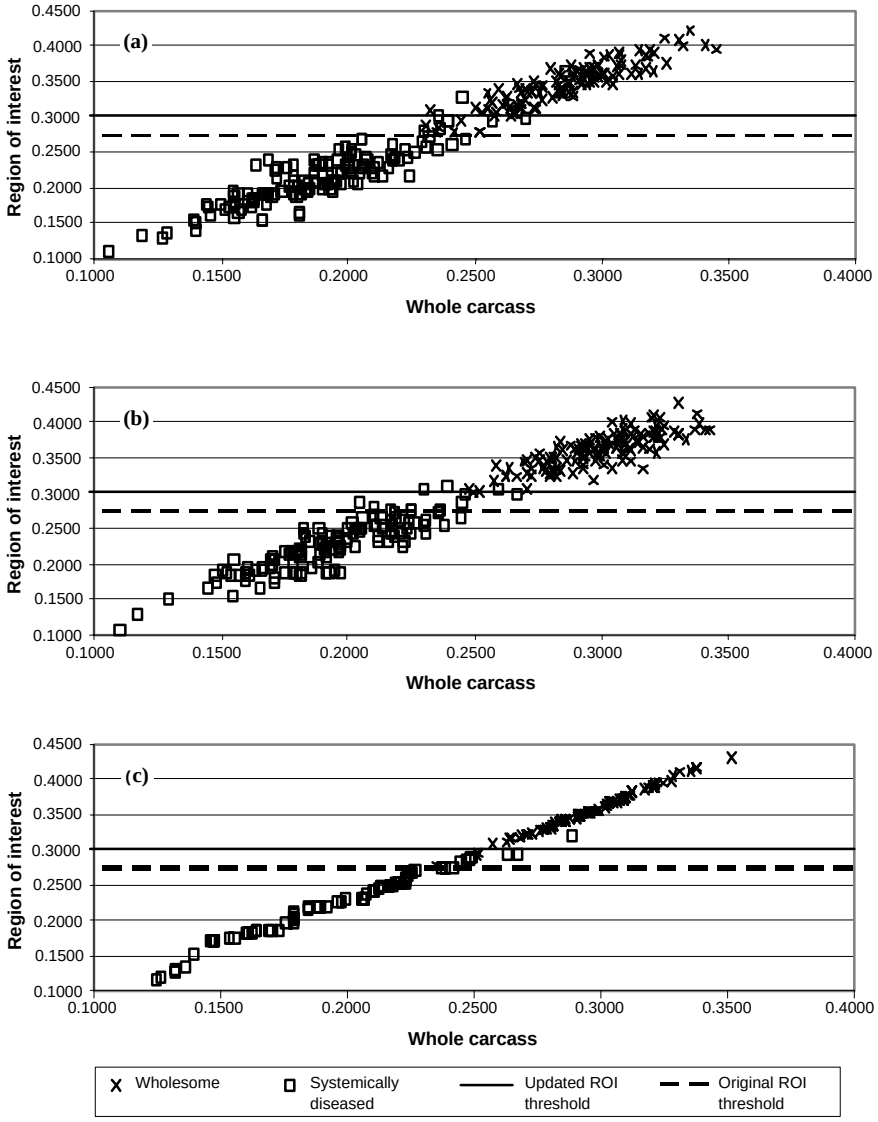

Figure 8. Average intensity values in the 580 nm waveband for (a) the first image batch, (b) the second image batch, and (c) the third image batch.

SUMMARY AND CONCLUSIONS

In this study, simple multispectral ROI features were developed to differentiate wholesome and systemically diseased chickens. Due to significant color differences between wholesome and systemically diseased chickens at 488, 540, and 580 nm, interference filters were selected at these wavebands for the multispectral imaging system; one additional filter was selected at 610 nm for image masking purposes. An algorithm was developed to find the ROI on the multispectral images. Differentiation thresholds for identifying wholesome and systemically diseased chickens were determined using a CART decision tree algorithm for 48 features per image that were defined by a combination of waveband, feature type, and classification area.

The AI_{540} and AI_{580} features in the ROI and WC areas were found capable of differentiating between wholesome and systemically diseased chicken images, while the AN and ADN features were not as effective in differentiation. It was observed that differentiation using the WC area was more sensitive to changes in the differentiation threshold. The AI_{540} feature achieved 96.3% and 97.1% accuracies in the ROI area for wholesome and systemically diseased chickens in the third batch, respectively, using thresholds determined from the combined first and second batch images. Similarly, the AI_{580} feature achieved 96.3% and 98.6% accuracies in the ROI area for wholesome and systemically diseased chickens, respectively, using thresholds determined from the combined first and second batch images. This differentiation method, using the simple calculation of average intensity, appears well suited for testing in an automated on−line multispectral inspection system.

REFERENCES

Breiman, L., J. H. Friedman, R. A. Olshen, and C. J. Stone. 1984. *Classification and Regression Trees.* Belmont, Cal.: Wadsworth.

Balk, B., and K. Elder. 2000. Combining binary decision tree and geostatistical methods to estimate snow distribution in a mountain watershed. *Water Resources Res.* 36(1): 13−26.

Chao, K., Y. R. Chen, W. R. Hruschka, and F. B. Gwozdz. 2002. On−line inspection of poultry carcasses by a dual−camera system. *J. Food Eng.* 51(3): 185−192.

Chao, K., Y. R. Chen, and D. E. Chan. 2003. Analysis of vis/NIR spectral variations of wholesome, septicemia, and cadaver chicken carcasses. *Applied Eng. in Agric.* 19(4): 453−458.

Chen, Y. R., and D. R. Massie. 1993. Visible/near−infrared reflectance and interactance spectroscopy for detection of abnormal poultry carcasses. *Trans. ASAE* 36(3): 863−869.

Eisenberg, J. N. S., and T. E. McKone. 1998. Decision tree method for the classification of chemical pollutants: Incorporation of across−chemical variability and within−chemical uncertainty. *Environ. Sci. and Tech.* 32(21): 3396−3404.

Liu, Y., and Y. R. Chen. 2000. Two−dimensional correlation spectroscopy study of visible and near−infrared spectral variations of chicken meats in cold storage. *Applied Spectroscopy* 54(10): 1458−1470.

Liu, Y., and Y. R. Chen. 2001. Analysis of visible reflectance spectra of stored, cooked, and diseased chicken meats. *Meat Science* 58(4): 395−401.

Park, B., K. C. Lawrence, W. R. Windham, and R. J. Buhr. 2002. Hyperspectral imaging for detecting fecal and ingesta contamination on poul‘try carcasses. *Trans. ASAE* 45(6): 2017−2026.

Pietersma, D., R. Lacroix, D. Lefebvre, and K. M. Wade. 2003. Performance analysis for machine−learning experiments using small data sets. *Computers and Electronics in Agric.* 38(1): 1−17.

Swatland, H. J. 1989. A review of meat spectrophotometry (300 to 800 nm). *Canadian Institute of Food Sci. and Tech. J.* 22: 390−402.

USDA. 1985. *Meat and Poultry Inspection*. Committee on the Scientific Basis of the Nation’s Meat and Poultry Inspection Program. Washington, D.C.: National Academy Press.

USDA. 1996. Pathogen reduction: Hazard analysis and critical control point (HACCP) systems. Final rule. *Fed. Reg.* 61: 28805−38855.

Windham, W. R., D. P. Smith, B. Park, K. C. Lawrence, and P. W. Feldner. 2003. Algorithm development with visible/near−infrared spectra for detection of poultry feces and ingesta. *Trans. ASAE* 46(6): 1733−1738.

Yang, C.−C., S. O. Prasher, and P. K. Goel. 2004. Differentiation of crop and weeds by decision−tree analysis of multi−spectral data. *Trans. ASAE* 47(3): 873−879.